

A coupled microwave-cavity system in the Rydberg-atom cavity detector for dark matter axions

M. Tada, Y. Kishimoto, M. Shibata, K. Kominato, I. Ogawa*,
H. Funahashi¹, K. Yamamoto², and S. Matsuki

Nuclear Science Division, Institute for Chemical Research, Kyoto University, Gokasho, Uji, Kyoto 611-0011, Japan

1 Department of Physics, Kyoto University, Kyoto 606-8503, Japan

2 Department of Nuclear Engineering, Kyoto University, Kyoto 606-8501, Japan

A coupled microwave-cavity system of cylindrical TM₀₁₀ single-mode has been developed to search for dark matter axions around 10 μeV (2.4 GHz) with the Rydberg-atom cavity detector at 10 mK range temperature. One component of the coupled cavity (conversion cavity) made of oxygen-free high-conductivity copper is used to convert an axion into a single photon with the Primakoff process in the strong magnetic field, while the other component (detection cavity) made of Nb is utilized to detect the converted photons with Rydberg atoms passed through it without magnetic field.

Top of the detection cavity is attached to the bottom flange of the mixing chamber of a dilution refrigerator, thus the whole cavity is cooled down to 10 mK range to reduce the background thermal blackbody-photons in the cavity.

The cavity resonant frequency is tunable over $\sim 15\%$ by moving dielectric rods inserted independently into each part of the cavities along the cylindrical axis. In order to reduce the heat load from the higher temperature side to the most cooled dilution refrigerator part, the tuning rod at the conversion cavity is especially driven via the Kevlar strings with a stepping motor outside the cryostat at room temperature.

The lowest temperature achieved up to now is 12 \sim 15 mK for the long period operation and the loaded Q value at low temperature is $3.5 \sim 4.5 \times 10^4$ for the whole range of frequency tuning. Characteristics and the performance of the coupled-cavity system are presented and discussed with possible future improvements.

I. INTRODUCTION

Disclosing the mystery of dark matter in the Universe is one of the most important and challenging issues in cosmology and particle physics [1]. A pseudo-scalar particle called axion is one of the most promising candidates for the cold dark matter. The axion was originally proposed to solve the so called "strong CP problem" in the QCD theory [2,3], thus being well motivated from the present particle physics. Astrophysical and cosmological analyses on the contribution of axions to the evolution of stars and also to the matter density of the Universe can constraint the mass of axions and the mass window still open now is from $\sim 10^{-3}\text{eV}$ to $\sim 10^{-6}\text{eV}$ [4,5]. From the theoretical analyses of axion productions in the early Universe, the most probable axion mass, assumed to be the dominant component of the dark matter, is suggested to be $\sim 10 \mu\text{eV}$.

One of the most efficient way to search for dark matter axions is to convert an axion into a single photon via the Primakoff process in a high quality-factor (Q) microwave cavity under the strong magnetic field and then to measure the excess microwave power in the cavity as a function of the cavity resonant frequency (corresponding to the mass of axions) [6]. Pioneering experiments along this line were first performed by Rochester-BNL-FNAL group [7] and then by Florida group [8] with a cryogenic microwave amplifier and the super-heterodyne method. The extension of the method has been further developed with a large scale superconducting magnet and a cavity system by a USA group [9].

We have developed a Rydberg-atom single-photon detector [10–12] for the dark matter axion search. The experimental principle of the method is schematically shown in Fig. 1. The axion-converted photons in the resonant cavity are absorbed by Rydberg atoms in a beam which are exclusively prepared to a lower state and the transition frequency of which to some upper state is approximately set equal to the cavity resonant frequency. Passed through, and just after exiting the cavity, the Rydberg atoms excited by absorbing photons are selectively ionized with the field ionization method [13]. Since the Rydberg atoms are prepared only to the lower state by the multistep laser excitation with narrow bandwidth single-mode lasers, this detection system is almost free from the inherent noise. Then the noise of this detection system and thus ultimate sensitivity is mainly determined by the background from the thermal blackbody radiations in the cavity which can be reduced by cooling the cavity and detection system as cold as possible with existing methods.

The essential requirements to be fulfilled for the detection system are thus the following: 1) the system should consist of coupled microwave cavities, one component of which is under the strong magnetic field, while the other component is free from the magnetic field in its inside to avoid its strong effect on the properties of the Rydberg atoms to be used. 2) the resonant frequency of the cavity should be continuously tunable over some range of frequency to be able to search for axions covering certain range of its mass. 3) the cavity and the detection system should be cooled enough to reduce the thermal blackbody photons from the cavity wall, possibly down to 10 mK range.

In addition to these fundamental requirements, the

quality factor (Q) should be as high as possible and also the conversion efficiency of axions into photons in the cavity should be as high as possible in order to make the efficiency of axion detection high enough.

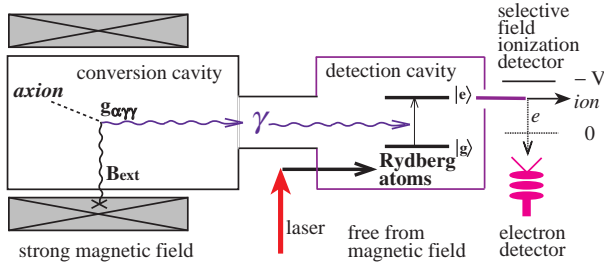


FIG. 1. Principle of the present experimental method to search for cosmic axions with Rydberg atoms in cooled resonant cavities. The axions are converted into photons in the conversion cavity permeated by a strong magnetic field, and then the converted photons are absorbed by the Rydberg atoms in the detection cavity which is free from the magnetic field. Only the excited Rydberg atoms are ionized and detected with the selective field ionization method. The cavities are cooled down to ~ 10 mK with a dilution refrigerator.

A pilot experimental apparatus of this line called CAR-RACK1 has been developed and is being used to search for dark matter axions at around 2.4 GHz (axion mass of $10 \mu\text{eV}$). To realize the above mentioned requirements actually, two single-mode cylindrical TM_{010} cavities are coupled through a ring-shape hole between them. One component of the coupled cavity is made of copper which is permeated by the strong magnetic field produced with a superconducting magnet and the other component is made of niobium to expel out the external magnetic field with the Meissner effect. Specifically the cavity system is attached to the bottom plate of the mixing chamber of a dilution refrigerator (DF) and thus the whole cavity and the adjacent detector components are cooled down to 10 mK range in order to reduce the thermal blackbody photons in the cavity. The cavity resonant frequency is tunable over $\sim 15\%$ by moving dielectric rods inserted independently in both cavity components along the cylindrical symmetry axis. In due course of the development, much attention has been especially paid to cool the system down to 10 mK range and also to get high Q cavities.

Although the present cavity system was constructed exclusively to be dedicated to search for dark matter axions, we believe that the underlying development of such system will also be useful to other kind of applications in general. In this note, the design principle and the actual apparatus of the present cavity system are described in sections 2 and 3. Then the characteristics and the performance of the system is presented and discussed in sections 4 and 5 with possible improvements in future. Section 6 is devoted to summarize the results of the present investigation.

II. DESIGN PRINCIPLE

A. General

Assuming the dark matter of our own galaxy (dark halo) consisting of axions, the number density of axions is given by

$$\bar{n}_a = 3.0 \times 10^{13} \left(\frac{\rho_a}{0.3 \text{ GeV cm}^{-3}} \right) \left(\frac{10^{-5} \text{ eV}}{m_a} \right), \quad (2.1)$$

where m_a is the mass of axion and the energy density of the cosmic axions ρ_a is taken to be equal to that of the galactic dark halo $\rho_{\text{halo}} \simeq 0.3 \text{ GeV cm}^{-3}$.

In the following we will firstly estimate the signal-to-background ratio (s/n) of axion detection in a very crude approximation without taking into account the quantum nature of the Rydberg-atom cavity detector. The pseudoscalar axion of spin-parity 0^- is converted to a photon in the strong magnetic field with the Primakoff process. The conversion rate in a resonant cavity is approximately given by [6]

$$R = \left(\frac{\epsilon_0}{\hbar^2} \right) g_{a\gamma\gamma}^2 \omega_c^{-1} Q_c B_0^2 G^2, \quad (2.2)$$

where $g_{a\gamma\gamma}$, ω_c , Q_c , B_0 , and G are the axion-photon coupling constant, the cavity resonant angular frequency, the cavity quality factor, maximum magnetic flux density and the geometric form factor of the cavity of order unity as described later in detail, respectively.

Taking into account the volume of the cavity, to be of order 10^3 cm^3 for axions with mass of $10 \mu\text{eV}$, the number of converted photons produced by the Primakoff process is estimated to be of order 0.1 to 1 from the above equations with conventionally available superconducting magnet. While this number seems to be significant, yet the background thermal photon number is much larger than this number even at 4 K temperature: In fact the mean number of thermal blackbody radiations \bar{n}_c present in a resonant single-mode cavity is given by

$$\bar{n}_c = \left(e^{\hbar\omega_c/k_B T_c} - 1 \right)^{-1}. \quad (2.3)$$

From this mean number, the number of background photons detected by a detector with effective Q value of Q_{det} is given by

$$N_d = \bar{n}_c \gamma_c \left(\frac{Q_{det}}{Q_c + Q_{det}} \right), \quad (2.4)$$

where γ_c is the dumping factor of the cavity given by

$$\gamma_c \equiv \frac{\omega_c}{Q_c} = 6.6 \times 10^5 \left(\frac{f_c}{2.4 \text{ GHz}} \right) \left(\frac{3 \times 10^4}{Q_c} \right). \quad (2.5)$$

The s/n ratio in a second is thus given approximately by

$$s/n \simeq O(1) \left(\frac{10\mu\text{eV}}{m_a} \right)^2 \left(\frac{Q_c}{3 \times 10^4} \right)^2 \left(\frac{B_0}{7\text{T}} \right)^2 \times \left(\frac{10^{5 \cdot (\frac{m_a}{10\mu\text{eV}})(\frac{10\text{mK}}{T})}}{10^5} \right), \quad (2.6)$$

where it is assumed that $k_B T \ll \hbar\omega_c$. From this equation, it is clear that the cavity has to be cooled down to 10 mK range if the s/n ratio is required to be of order better than one.

B. Quantum treatment of axion - photon - Rydberg-atom interactions in resonant cavities

Although the above analyses are useful for the very crude estimation of the detection efficiency, more rigorous analyses have to be based on the quantum theory of axion-photon-atom interactions as clarified previously [11,14,15] in detail. Theoretical analyses are briefly discussed in the following.

The axion-photon interaction under a strong static magnetic field with flux density \mathbf{B}_0 is described by the Lagrangian density

$$\mathcal{L}_a = \hbar^{1/2} \epsilon_0 g_{a\gamma\gamma} \phi \mathbf{E} \cdot \mathbf{B}_0, \quad (2.7)$$

where $\hbar^{1/2}$ and ϵ_0 (dielectric constant) are explicitly factored out so that the Lagrangian density has the right dimension $\mathcal{L}_a \sim \hbar s^{-1} m^{-3} \sim \text{eV m}^{-3}$ with the axion-photon-photon coupling constant $g_{a\gamma\gamma} \sim \text{eV}^{-1}$. The axion-photon-photon coupling constant is calculated [2,3,16] as

$$g_{a\gamma\gamma} = c_{a\gamma\gamma} \frac{\alpha}{2\pi^2} \frac{m_a}{f_\pi m_\pi} \frac{(1+Z)}{\sqrt{Z}}, \quad (2.8)$$

where $Z = m_u/m_d$, and

$$c_{a\gamma\gamma} = \frac{D}{C} - \frac{2(4+Z)}{3(1+Z)} \quad (2.9)$$

with

$$D = \text{Tr} Q_{\text{PQ}} Q_{\text{em}}^2, \quad C \delta_{ab} = \text{Tr} Q_{\text{PQ}} \lambda_a \lambda_b. \quad (2.10)$$

The parameter $c_{a\gamma\gamma}$ represents the variation of the axion-photon-photon coupling depending on the respective Peccei-Quinn models such as the so-called KSVZ and DFSZ [3].

The electric field operator in the cavity \mathcal{V} is given by

$$\mathbf{E}(\mathbf{x}, t) = (\hbar\omega_c/2\epsilon_0)^{1/2} [\boldsymbol{\alpha}(\mathbf{x})c(t) + \boldsymbol{\alpha}^*(\mathbf{x})c^\dagger(t)] \quad (2.11)$$

for the radiation mode with a resonant frequency ω_c , where ϵ_0 is the dielectric constant. The creation and annihilation operators satisfy the usual commutation relation

$$[c, c^\dagger] = 1. \quad (2.12)$$

The mode vector field $\boldsymbol{\alpha}(\mathbf{x})$ is normalized by the condition

$$\int_{\mathcal{V}} |\boldsymbol{\alpha}(\mathbf{x})|^2 d^3x = 1. \quad (2.13)$$

The whole cavity \mathcal{V} may be viewed as a combination of two subcavities, the conversion cavity \mathcal{V}_1 with volume V_1 and the detection cavity \mathcal{V}_2 with volume V_2 , which are coupled together:

$$\mathcal{V} = \mathcal{V}_1 \oplus \mathcal{V}_2. \quad (2.14)$$

The axion-photon conversion takes place in \mathcal{V}_1 under the strong magnetic field, while the Rydberg atoms are excited by absorbing the photons in \mathcal{V}_2 . It is then suitable to divide the mode vector as

$$\boldsymbol{\alpha}(\mathbf{x}) = \boldsymbol{\alpha}_1(\mathbf{x}) + \boldsymbol{\alpha}_2(\mathbf{x}), \quad (2.15)$$

where $\boldsymbol{\alpha}_1(\mathbf{x}) = \mathbf{0}$ for $\mathbf{x} \in \mathcal{V}_2$ and $\boldsymbol{\alpha}_2(\mathbf{x}) = \mathbf{0}$ for $\mathbf{x} \in \mathcal{V}_1$, respectively. The normalization condition of $\boldsymbol{\alpha}(\mathbf{x})$ is rewritten as

$$\int_{\mathcal{V}_1} |\boldsymbol{\alpha}_1(\mathbf{x})|^2 d^3x + \int_{\mathcal{V}_2} |\boldsymbol{\alpha}_2(\mathbf{x})|^2 d^3x = 1. \quad (2.16)$$

The actual cavity is designed so that neglecting the small joint region the subcavities \mathcal{V}_1 and \mathcal{V}_2 admit the mode vectors $\boldsymbol{\alpha}_1^0(\mathbf{x})$ and $\boldsymbol{\alpha}_2^0(\mathbf{x})$ (up to the normalization and complex phase), respectively, whose frequencies are tuned to be almost equal to some common value ω_c^0 . In this situation, as confirmed by numerical calculations and experimental observations, two nearby eigenmodes with the frequencies $\omega_c, \omega'_c \simeq \omega_c^0$ are obtained for the whole cavity \mathcal{V} . Then, the mode vector $\boldsymbol{\alpha}(\mathbf{x})$ is constructed approximately of $\boldsymbol{\alpha}_1(\mathbf{x}) \simeq \boldsymbol{\alpha}_1^0(\mathbf{x})$ and $\boldsymbol{\alpha}_2(\mathbf{x}) \simeq \boldsymbol{\alpha}_2^0(\mathbf{x})$ with significant magnitudes in both \mathcal{V}_1 and \mathcal{V}_2 . The conversion of the cosmic axions takes place predominantly to the radiation mode which is resonant with the axions satisfying the condition $|\omega_c - m_a/\hbar| \lesssim \gamma_a$ (axion width) \sim small fraction of γ_c (cavity damping rate). The cavity can be designed so as to give a sufficient separation of $|\omega_c - \omega'_c| >$ several γ_c for the nearby modes with strong coupling between \mathcal{V}_1 and \mathcal{V}_2 . Therefore, in the search for the signal from the cosmic axions, the one resonant mode can be extracted solely for the electric field in a good approximation, as given in Eq. (2.11), whose frequency ω_c is supposed to be close enough to the axion frequency $\omega_a = m_a/\hbar$.

The original Lagrangian density for the axion-photon-photon coupling in Eq. (2.7) provides the effective interaction Hamiltonian between the coherent axion mode a and the resonant radiation mode c ,

$$H_{ac} = \hbar\kappa(a^\dagger c + ac^\dagger). \quad (2.17)$$

The coherent axion mode can be identified as

$$a(t) = \Sigma_a^{-1/2} \int_{\mathcal{R}_a} \frac{d^3k}{(2\pi)^3 2\omega_k} a_{\mathbf{k}}(t). \quad (2.18)$$

where R_a represents the coherent region of axions, and the normalization factor is given by

$$\Sigma_a = \int_{\mathcal{R}_a} \frac{d^3k}{(2\pi)^3 2\omega_k} \equiv \frac{1}{2m_a} \left(\frac{\beta_a m_a}{2\pi\hbar} \right)^3, \quad (2.19)$$

so that the coherent mode operator satisfies the canonical commutation relation,

$$[a, a^\dagger] = 1. \quad (2.20)$$

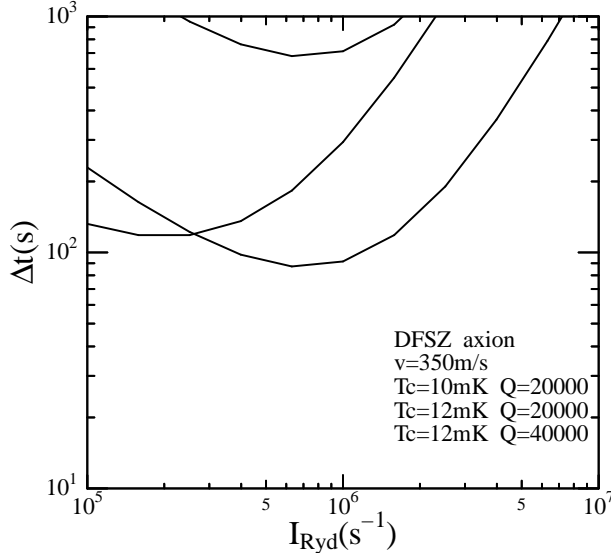


FIG. 2. Necessary time to observe the axion-converted photon signals in 3σ level as a function of the average number of Rydberg atoms in resonant cavity under the existence of the background thermal blackbody photons. The axion-converted photon signals are estimated from the DFSZ axion model.

The axion-photon conversion in the cavity \mathcal{V}_1 is well described with this interaction Hamiltonian. The coupling constant κ is determined for $\omega_c \simeq m_a/\hbar$ [2,3,16]

$$\begin{aligned} \kappa &= \hbar^{1/2} g_{a\gamma\gamma} \epsilon_0^{1/2} B_{\text{eff}} \left[\left(\frac{\beta_a m_a}{2\pi\hbar} \right)^3 \frac{V_1}{2} \right]^{1/2} \\ &= 4 \times 10^{-26} \text{eV}\hbar^{-1} \left(\frac{g_{a\gamma\gamma}}{1.4 \times 10^{-15} \text{GeV}^{-1}} \right) \left(\frac{B_{\text{eff}}}{4\text{T}} \right) \\ &\times \left(\frac{\beta_a m_a}{10^{-3} \times 10^{-5} \text{eV}} \right)^{3/2} \left(\frac{V_1}{5000 \text{cm}^3} \right)^{1/2}, \quad (2.21) \end{aligned}$$

where

$$B_{\text{eff}} = \zeta_1 G B_0, \quad (2.22)$$

and B_0 is the maximal density of the external magnetic flux. The axion-photon-photon coupling constant $g_{a\gamma\gamma}$ is taken here to be the value expected from the DFSZ axion model [3] at $m_a = 10^{-5} \text{eV}$.

The form factor for the magnetic field is given by

$$G = \zeta_1^{-1} V_1^{-1/2} \left| \int_{\mathcal{V}_1} d^3x \alpha_1(\mathbf{x}) \cdot [\mathbf{B}_0(\mathbf{x})/B_0] \right| \quad (2.23)$$

with

$$\zeta_1 = \left[\int_{\mathcal{V}_1} d^3x |\alpha_1(\mathbf{x})|^2 \right]^{1/2}. \quad (2.24)$$

This additional factor ζ_1 (< 1 as seen from Eq.(2.16)) represents the effective reduction of the axion-photon conversion which is due to the fact that the magnetic field is applied only in the conversion cavity \mathcal{V}_1 . We may obtain, for example, the effective magnetic field strength $B_{\text{eff}} \simeq 4\text{T}$, as taken in Eq.(2.21), by using typically a magnet of $B_0 \simeq 7\text{T}$ and the cavity system with $G = \sqrt{0.7}$ of TM_{010} mode and $\zeta_1 \simeq 0.7$ for the conversion cavity. The actual value of B_{eff} was evaluated with the calculated electric field distributions in the cavity as described in detail later.

Now the time evolution of the axion - photon - Rydberg-atom system is governed by the following equations of motion in the Heisenberg picture, when all of the Rydberg atoms are prepared initially in the lower state [11,14,15]:

$$\frac{dz_i}{dt} = K_{ij} z_j + F_i, \quad (2.25)$$

where $z_i = (b, c, a)$, $F_i = (0, F_c, F_a)$, and

$$K = \begin{pmatrix} -i\omega_b & i\Omega_N & 0 \\ i\Omega_N & -i\omega_c - \frac{1}{2}\gamma_c & i\kappa \\ 0 & i\kappa & -i\omega_a - \frac{1}{2}\gamma_a \end{pmatrix} \quad (2.26)$$

with $\gamma_a \simeq \beta_a^2 m_a$, the energy dispersion of the cosmic axions. The operators a, b , and c refer to axion, atom and cavity-mode photon, respectively. The external forces F_c and F_a are introduced for the Liouvillian relaxations of the photons and axions, respectively [17,18].

By solving the equations, the detection efficiency can be numerically calculated as a function of various experimental parameters such as the transit time of the atomic beam in the detection cavity, cavity temperature and the number of Rydberg atoms passed through the cavity. From these results the optimum condition of the experimental parameters like the transit time of the Rydberg atoms, or the velocity of the atoms can be determined. The cavity system was thus designed to meet these requirement.

Along the line of these analyses, further refined treatment of the system has been recently performed by taking into account the spatial distribution of the Rydberg atoms in the cavity and also the actual electric field distribution along the path of the atoms in the cavity. The resulting modifications were also taken into account for the design of the cavity system, although the modifications are not profound [14,15].

Specifically the most important ingredient among these parameters is the average number of Rydberg

atoms present in the cavity. Due to the collective interactions of the atoms with the cavity mode, the overall coupling strength is proportional to the square of the number of atoms in the cavity so that the most optimum coupling strength can be tuned by adjusting the injecting number of Rydberg atoms, thus with the oven temperature of thermal atomic beam and/or with the power of the second laser.

Typical dependence of the necessary time to search for axions over 10 % region with 3σ level on the number of the Rydberg atoms are shown in Fig. 2. From this dependence it is found that the optimum number of Rydberg atoms should be around $5 \times 10^5 \text{sec}^{-1}$ for the 10 μeV axions with the mean atomic velocity of 350 m/sec.

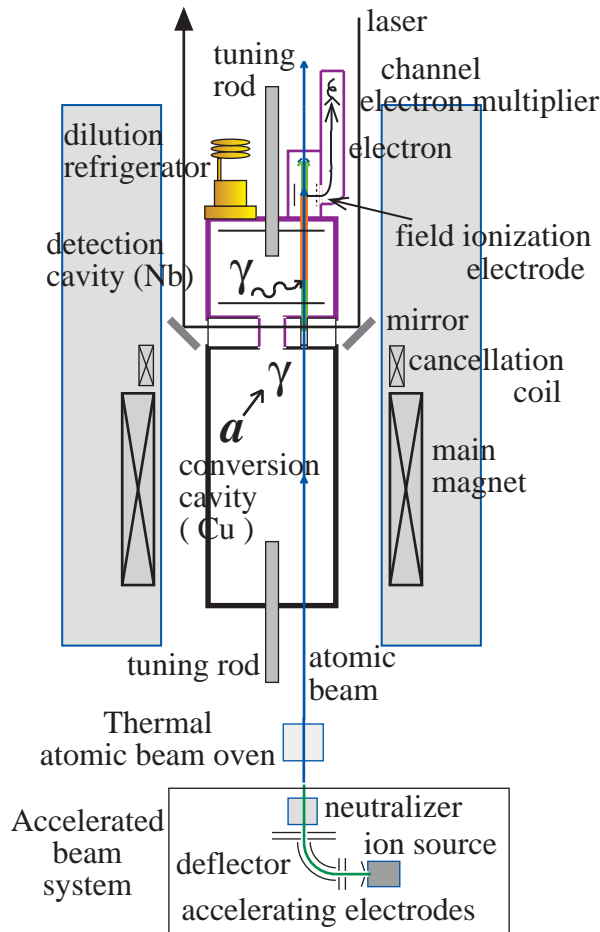


FIG. 3. Schematic diagram of the present experimental system to search for cosmic axions with Rydberg atoms in cooled resonant cavities. The cavities and the related detector system are all cooled down to ~ 10 mK with a dilution refrigerator to reduce the thermal blackbody photons. Accelerated or thermally produced atomic beam of Rb in its ground state is utilized for the Rydberg atoms.

C. Rydberg-atom cavity detector

Following the above theoretical analyses of the optimum setup of the experimental system, the whole system of the present axion search apparatus was designed as schematically shown in Fig. 3. Thermal or accelerated atomic beam, produced from a thermal Rb oven placed beneath the cryostat, are injected into the low temperature cavity and stopped at 1K-pot plate of the dilution refrigerator system after passing through the detection cavity. Just in front of the detection cavity the ground state atoms of ^{85}Rb are excited to a Rydberg state with 2- or 3-step laser excitation. Laser beams are introduced from the top into the cryostat and after interacting with atoms are then extracted outside through a glass window.

The Rydberg atoms excited to an upper state are ionized at the field ionization electrode and the electrons thus produced are guided through a series of focussing ring-electrodes to, and detected with, a channeltron electron multiplier placed at the 1K-pot plate. The whole cavity and the field ionization detection system are cooled down to 10 mK range with the DF. For this purpose the top of the detection cavity is attached to the bottom plate of the mixing chamber.

III. APPARATUS

The whole coupled-cavity system is shown in Fig. 4.

The cavity system is located in the inner vacuum chamber surrounded by a liquid He bath, a liquid nitrogen bath and a outer vacuum chamber.

Two TM_{010} single-mode cavities of the same inner diameter are connected to each other through a ring-shape hole. The resonant frequency of the cylindrical TM_{010} cavity is determined by its diameter D as

$$f_c \equiv \frac{\omega_c}{2\pi} = 2.55 \text{GHz} \left(\frac{90 \text{mm}}{D} \right). \quad (3.1)$$

Two cavity components are made of oxygen-free high-conductivity copper OFHC (conversion cavity) and niobium (detection cavity), respectively. The detection cavity is made of superconducting niobium to expel out the external magnetic field with the Meissner effect.

The tuning of the cavity resonant frequency is accomplished by inserting and moving dielectric rods in both the conversion and the detection cavities along the cylindrical symmetry axis. This choice of the tuning method was adopted from its simple mechanism of driving from the outside of the cryostat with stepping motors, although the form factor of the cavity is not the best. The rod for the detection cavity is driven from the top of the cryostat, while that for the conversion cavity is driven from the bottom of the cryostat.

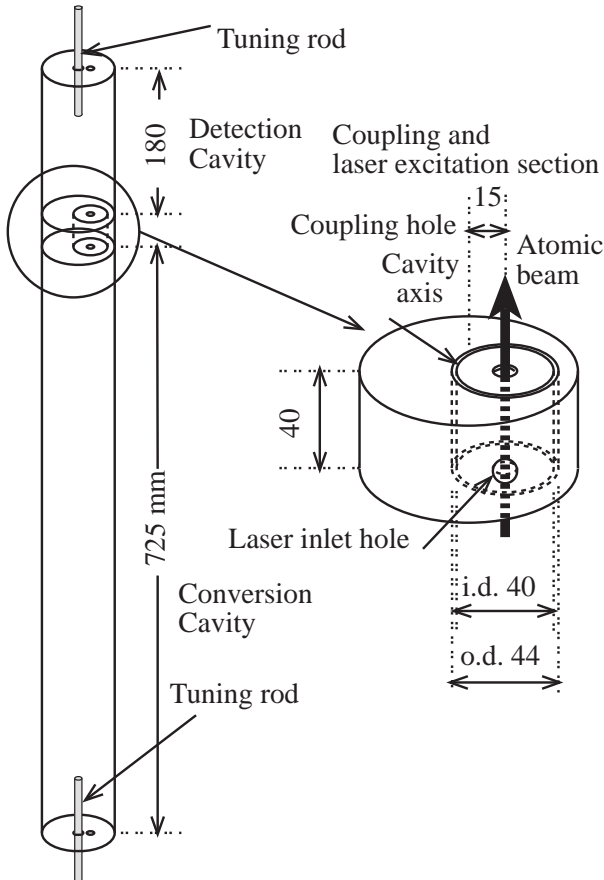


FIG. 4. Coupled cavity and coupling structure in the present cavity system.

A. coupled cavity

The two cavity components are coupled through a ring-shape hole as shown in Fig. 4. The strength of the coupling can be estimated by the frequency separation of the two eigen modes. This separation is related to how fast the stored power in one component of the cavity is transferred to another component. This frequency separation was estimated with a two-dimensional computer code SUPERFISH for alternating electromagnetic field calculations. The field distribution in the cavity is affected by the inserted rod position, due to the large dielectric constant of the rod material. Although the electric field direction is not always perfectly parallel to the cylindrical axis, the whole field distribution is consistent with the TM_{010} mode for the full range of the frequency as a function of the rod position.

One of the eigen mode (parallel mode) has an electric field directions in parallel for both components, while in the other eigen mode (anti-parallel mode), the field direction of the conversion cavity is anti-parallel to that of the detection cavity. The electric field in the anti-parallel mode is stronger in the conversion cavity than in the detection cavity, while opposite situation is realized

in the parallel mode.

The anti-parallel eigen mode, in which the electric field in the conversion cavity is stronger, was chosen for the actual cavity system in the present case.

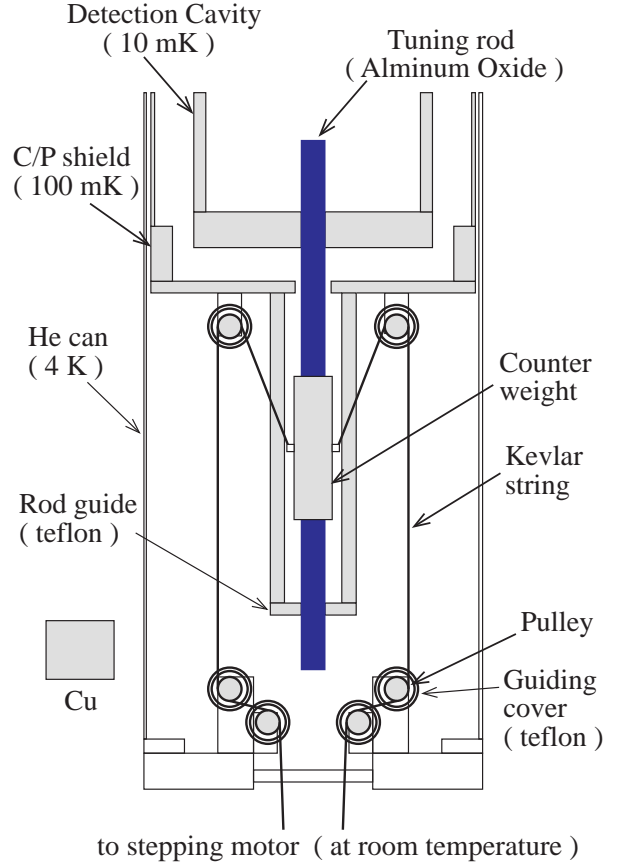


FIG. 5. Schematic drawing of the driving mechanism of the rod in the conversion cavity with Kevlar strings for frequency tuning. The strings are moved by a stepping motor outside the cryostat at room temperature.

B. Frequency tuning

The frequency tuning is accomplished by inserting the dielectric rods to both the detection and conversion cavities along the cylindrical axis. Depending on the size of the inner diameter of the cavity, the diameter of the tuning rod is determined for the resonant frequency to cover the expected frequency regions. Aluminum-oxide rod of 7 mm diameter is used for both cavities.

Since the cavity is cooled down to 10 mK range, heat leak from the higher temperature side is extremely important. For the detection cavity, which is located at the upper part of the cavity system and attached to the bottom plate of the mixing chamber, the rod is inserted to the cavity through a stainless-steel pipe and a TI-polymer pipe [19] from the top of the cryostat. The rod was anchored to the liquid nitrogen shield plate, liquid He can, and then to the cold plate shield (c/p shield plate) at

~ 100 mK temperature with a strand of copper meshes.

Only the c/p shield at 100 mK is available for the rod of the conversion cavity to be anchored so that special care has to be taken to avoid the heat leak from the room temperature side coming into the cavity at 10 mK range. The lower-side rod for the conversion cavity is thus moved via Kevlar strings [19] with a stepping motor outside the cryostat at room temperature. The driving mechanism is shown schematically in Fig. 5. The Kevlar string has quite low heat conductivity and still has enough strength to drive the rod of weight ~ 100 g. It has also quite low extensibility. The heat leak from the room temperature parts is estimated to be less than 50 nW.

C. Magnetic field shielding

Although we need strong magnetic field in the conversion cavity, it is easier to handle the Rydberg-atom single-photon detector in a circumstance without magnetic field to avoid the magnetic field in the detection cavity, because otherwise we have a complicated energy levels of the Rydberg states due to the effect of the Zeeman splitting. To expel out the strong magnetic field from the detection cavity, following method was adopted in the region of the detection cavity: first, the external magnetic field at the detection cavity was reduced to less than 0.09 T with a superconducting coil (cancellation coil) with counter flow of the current against the main magnet coil. Second, the detection cavity and the coupling part are made of Nb metal, which become a superconducting state at the cooled stage, thus the inner field being expelled out due to the Meissner effect.

It is noted here that in order to well realize the field free region in the detection cavity, we have to carefully take into account the effect of the demagnetization field induced by the superconducting Nb metals. With a three-dimensional eddy current program EDDY [20], the magnetic flux density resulting from the insertion of the superconducting Nb metals was calculated and the proper shape of the Nb cavity were thus designed to expel the flux density out of the detection cavity. The detailed treatment of the magnetic shield will be reported elsewhere.

D. Selective-field-ionization detector

Selective field ionization detector consists of three parts; field ionization electrodes, transport electrodes for the ionized electrons and the electron multiplier for detecting the electrons. The field ionization electrodes are located in the Nb box set at the bottom plate of the mixing chamber and the Rydberg atoms entered into the electrodes after passing through the detection cavity. The ionized electrons are then transported into the electron multiplier located at the 1K-pot plate through

the number of ring electrodes for focussing. These transport electrodes are distributed from the vicinity of the ionization electrodes to the 1K-pot region through the cold/plate region to effectively transport the electrons.

These configurations are adopted to keep the cavity and the field ionization parts as cool as possible, since the used channel electron multiplier produces heat power as large as 10 mW. Moreover the channeltron multiplier can not be used at such low temperature as 10 mK range, because the amplification gain is strongly reduced at such low temperature. Therefore the channeltron multiplier has to be always kept at temperature higher than 20 K. In order to fulfill this requirement, the multiplier was heated up with a heating coil surrounding it and separated thermally from the 1K-pot plate by supporting it with a low thermal conductivity dielectric material called TI polymer. The introduced power of the heating coil is about 30 mW and the current flowing between the top and the collector electrodes of the channeltron multiplier is about $5 \mu\text{A}$. Detailed description of the SFI detector will be published elsewhere.

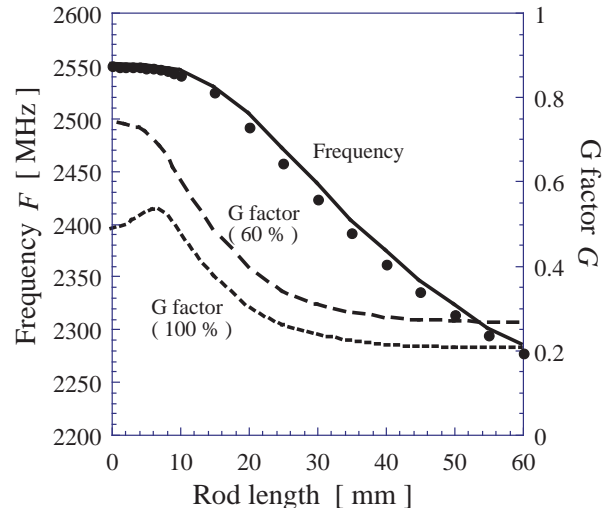


FIG. 6. Frequency and form-factor variation with the position of the tuning rod in the conversion cavity. Solid line is the calculated frequency variation and the solid circles show the observed results. Also shown is the G factor with (labeled 60% in the Figure where 40% of the cavity at the lower part is cut off for the estimation) and without (denoted 100%) taking into account the lower part of the conversion cavity. See text in detail for the treatment of the lower part of the cavity.

E. Associated equipment

In addition to the coupling hole between the two sub-cavities and the holes for the frequency tuning rod, each cavity has also a hole to introduce the Rydberg atomic beam into the cavity and to make the atoms pass through for detecting the excited atoms with the field ionization method. These holes have some effect on the degradation of the loaded Q value of the cavity.

Several associated equipments were also installed to the cavity system. One is the electrodes for inducing the Stark shift of the Rydberg states inserted along the beam path in the cavity. The electrodes are used to tune finely the Rydberg-atom transition frequency to match with the cavity resonant frequency and thus to be able to search for axions over some range of axion mass. The detailed structure of the Stark electrodes will be reported elsewhere.

Since the total length of the whole cavity system is 80 cm, some acoustic vibrational motion may possibly be induced at the lower part of the cavity. In order to avoid this vibration, the lower part of the cavity were connected to the c/p cylindrical shield plate with several small graphite rods. The induced heat leak from the c/p shield to the cavity is negligible due to the low thermal heat conductivity of the graphite used.

IV. PERFORMANCE

A. frequency tuning and the Q value

The cavity resonant frequency was measured with a tracking analysis system in the ADVANTEST R3261A spectrum analyzer. The coupling antenna in both the cavity components are straight thin wire of about 1 mm length. Semi-rigid UT141 cables made of Be/Cu were used to connect the antenna to the main amplifier outside of the cryostat. In cooled stage, a cryogenic amplifier and a circulator inserted between the cavity and the main amplifier outside the cryostat were used to increase the sensitivity for the calibration. However once the calibration measurement has been finished, these auxiliary equipments were removed, since they induce some noise into the cavity system and thus degrade the performance of the present Rydberg-atom cavity detector.

The tuning of the cavity resonant frequency was controlled by varying the position of the rod in the cavity with a stepping motor through a computer. A data acquisition and control program LabVIEW was used for the whole control of the tuning system. It is noted that the tuning of the CC rod position is mostly effective for the cavity frequency tuning and is not so sensitive to the DC rod position. It is therefore not necessary for the tuning to finely adjust the positions of the two rods relatively to each other.

The measured frequency range covered by the tuning rod is shown in Fig. 6 together with the calculated result for comparison. Although the extensibility of the strings used is quite small, the effect of backlash of the stepping motors has some effect of the reproducibility of the resonant frequencies when back and forth movement has been made. However these backlash effect can be avoided by always moving the rod to the same direction during the course of the experiment.

The loaded Q value observed is $3.5 \sim 4.5 \times 10^4$ for the whole range of the resonant frequencies tuned. The Q value achieved is quite sensitive to the goodness of the contact between the side cylinder and the upper and the lower plates. In between them we inserted and tightened thin indium wires and/or thin copper rings which have especially sharp edges on both side of the connecting surfaces. Both methods worked well, although the use of copper rings is more flexible in practice.

The stability of the resonant frequency for a long period is one of the important factors for the present purpose of the experiment. We checked the stability of the frequency by fixing the rod position. It was found that the resonant frequency is stable within 3 kHz for more than 3 hours, enough stability for the present purpose.

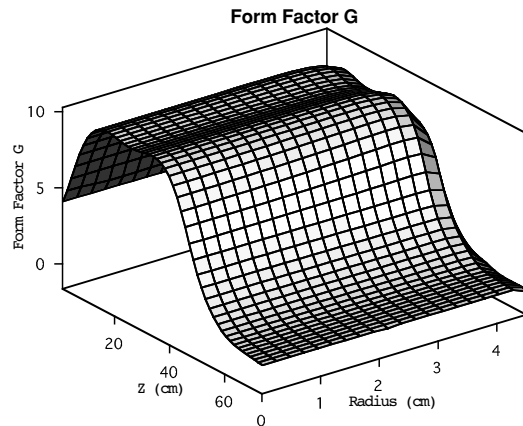


FIG. 7. Distribution of form factor G in the present cylindrical TM_{010} cavity.

B. Conversion form-factor

The form factor for the axion conversion is proportional to $E\dot{B}$ as described in the previous section. In Fig. 6 shown is the form factor G evaluated from the electric field distribution in the cavity with the code SUPERFISH. The magnetic field in the cavity is calculated from the superconducting coil dimensions with the program POISSON.

The distribution of the G factor in the cavity is shown in Fig. 7 in three dimensional representation. The distribution along the symmetry z axis is mainly due to that of the magnetic field.

It is noted that from the view point of maximum G -factor attainable, there should be some optimum value for the length of the conversion cavity. However due to the requirement of the effective coupling to the detection cavity, the conversion cavity is inevitably longer than the optimum value. This longer cavity apparently results in smaller effective magnetic field B_{eff} due to the weak magnetic field near the detection cavity region. However actually this does not mean any serious deterioration of

the detection sensitivity, since this effect of longer cavity has been taken into account from the first design stage.

The only drawback of this longer cavity is that we have many series of higher TE modes which cross to the fundamental TM mode as we tune the frequency of the cavity, thus losing many frequency bands due to the avoided crossings. By using another rod with different diameter, however, we can fill these empty space in the frequency sweep, since the different rod brings avoid crossings at different frequencies.

C. Cooling

The temperature at the mixing chamber and the cavity was measured with the anisotropy distribution of gamma rays from an oriented ^{60}Co single crystal source. A thermometer of RuO_2 was also used for the temperature measurements at several places on the cavity surface. The weight of the cavity system is about 25 kg and it takes sometime to cool the whole cavity system down enough to 10 mK range. In Fig. 8 shown is the cooling characteristics of the cavity system with time after the pumping of the $^3\text{He}/^4\text{He}$ mixture gas was started. It takes about 5 hours for the whole system to be cooled down to 12 mK.

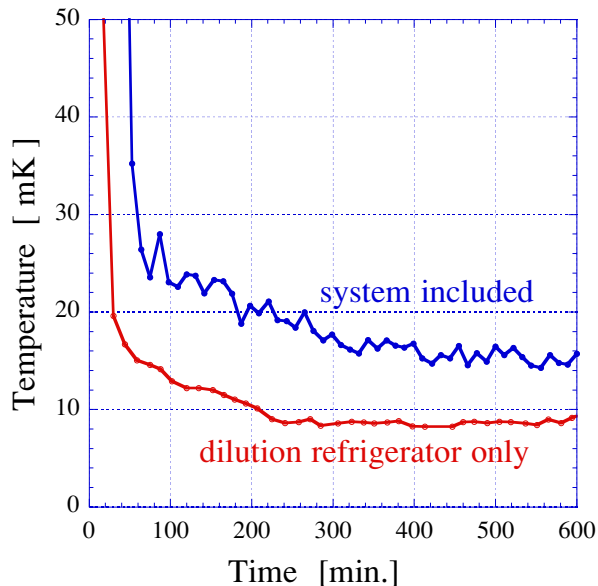


FIG. 8. Cooling rate of the present cavity system with a dilution refrigerator. The time zero represents when the roots pump is on.

V. DISCUSSION

The system has fairly satisfactory performance for the present purpose of the axion search experiment. The temperature achieved for the cavity is $12 \sim 15$ mK. This could be further improved by reducing the heat leak from the higher temperature side.

The estimated Q value of the cavity from the surface resistance of the materials used is approximately given by

$$Q_c \sim 1.3 \times 10^5 \left(\frac{f_c}{1\text{GHz}} \right)^{-2/3}. \quad (5.1)$$

The actual Q achieved in the present system is somewhat lower than the value estimated from this tendency. This lower Q value may be due to many holes drilled and the associated equipment installed in the cavity such as the Stark plate electrodes in the cavity. Detailed analyses on this point, however, have not yet been tried.

The form factor G of the present magnet and the cavity system seems to be rather small even at the lower frequency region where the insertion length of the rod is rather small. As discussed already, this lower value is, however, mainly due to the long length of the cavity, in which the magnetic field at the lower section is quite small, because of the effect of the cancellation magnet. If we neglect the contribution of the lower part of the cavity in the evaluation of the effective magnetic field, then the resulting values of G are improved as shown also in Fig. 6.

Further improvement on the value of the form factor may be possible by adopting the metal/dielectric post system in replace of the present rods. Unfortunately this improvement is difficult in the present structure of the cryostat, because no useful space is available at the mixing chamber region where we have to install a selective field ionization detector and microwave power input circuitry to the cavity. However in a new large scale apparatus called CARRACK2 [21], we developed a new cryostat system in which the detection cavity is set at the lower side and the laser and the atomic beam are introduced horizontally through the lower part of the vacuum chamber, thus enabling us to install the post driving system for the tuning of the cavity frequency. This development will be reported elsewhere.

VI. SUMMARY

We have developed the coupled cavity system for the dark matter axion search with the Rydberg-atom cavity detector. In order to fulfill the necessary ingredients of the Rydberg-atom cavity detector, one of the component of the OFHC-copper cavity (conversion cavity) is permeated by the strong magnetic field, while the other component (detection cavity) was arranged to be free from the external magnetic field. The detection cavity is made of superconducting Nb, with which the external magnetic field is expelled out to fulfill the above requirement.

The conversion cavity is attached to the bottom plate of the mixing chamber of the dilution refrigerator and thus the whole system is cooled down to 10 mK range. Great care was taken to reduce the heat load from the higher temperature side through the tuning rods driven

from the cryostat outside at room temperature. Especially Kevlar string of low heat conductivity was used to access the tuning rod from the outside. The minimum temperature achieved is 12 mK, and the loaded Q value obtained is $3.5 \sim 4.5 \times 10^4$ for the whole range of the frequency tuning of about 15 %.

ACKNOWLEDGMENTS

The authors would like to thank A. Masaike for his continuous encouragement throughout this work. They are also indebted to S. Takeuchi of JAERI, Tokai for giving us invaluable information on the Nb cavity fabrications. This research was partly supported by a Grant-in-Aid for Specially Promoted Research (No. 09102010) by the Ministry of Education, Science, Sports, and Culture (Monbusho), Japan.

- [15] A. Kitagawa, K. Yamamoto and S. Matsuki, LANL-Preprint-Archive hep-ph/9908445, submitted to Phys. Rev. D.
- [16] D. B. Kaplan, Nucl. Phys. B **260**, 215 (1985); M. Srednicki, Nucl. Phys. B **260**, 689 (1985).
- [17] S. Haroche and J. M. Raimond, *Advances in Atomic and Molecular Physics* **20**, 347, edited by D. Bates and B. Bederson (Academic, New York, 1985); S. Haroche, *Fundamental Systems in Quantum Optics*, Les Houches 1990 LIII, p.767 (North-Holland, Amsterdam, 1992).
- [18] See for example, W.H. Louisell, *Quantum Statistical Properties of Radiation*, (John Willey and Sons, New York, 1990).
- [19] Made of Toray *co.*, Ltd. in Japan.
- [20] Software system made of Photon *co.*, Ltd. in Japan.
- [21] M. Tada *et al.*, Nucl. Phys. **72B**, 164 (1999).

* Present address: Department of Physics, Osaka University, Toyonaka, Osaka 560-0043, Japan

- [1] Recent reviews include *Proceedings of the Second International Workshop on the Identification of Dark Matter in the Universe*, eds. N. J. C. Spooner and V. Kudryavtsev, (World Scientific, Singapore, 1999).
- [2] R. D. Peccei and H. R. Quinn, Phys. Rev. Lett. **38**, 1440 (1977); Phys. Rev. D **16**, 1791 (1977); S. Weinberg, Phys. Rev. Lett. **40**, 223 (1978); F. Wilczek, Phys. Rev. Lett. **40**, 279 (1978).
- [3] J. -E. Kim, Phys. Rev. Lett. **43**, 103 (1979); M. A. Shifman, A. I. Vainshtein and V. I. Zakharov, Nucl. Phys. **B166**, 493 (1980); A. R. Zhitnitsky, Sov. J. Nucl. Phys. **31**, 260 (1980); M. Dine, W. Fischler and M. Srednicki, Phys. Lett. **104B**, 199 (1981).
- [4] Recent reviews include G. Raffelt, Phys. Rep. **198**, 1 (1990) .
- [5] Recent reviews include E. Kolb and M. Turner, *The Early Universe*, (Addison-Wesley, New York, 1990).
- [6] P. Sikivie, Phys. Rev. Lett. **51**, 1415 (1983) ; Phys. Rev. **D32**, 2988 (1985) ; L. Krauss et al., Phys. Rev. Lett. **55**, 1797 (1985) .
- [7] S. de Panfillis *et al.*, Phys. Rev. Lett. **59**, 839 (1987) ; W.U. Wuensch *et al.*, Phys. Rev. D **40**, 3153 (1989) .
- [8] C. Hagmann *et al.*, Phys. Rev. D **42**, 1297 (1990) .
- [9] C. Hagmann et al., Phys. Rev. Lett. **80**, 2043 (1998).
- [10] S. Matsuki and K. Yamamoto, Phys. Lett. **263B**, 523 (1991) .
- [11] I. Ogawa, S. Matsuki and K. Yamamoto, Phys. Rev. **D42** 1297 (1990) .
- [12] S. Matsuki et al., Nucl. Phys. **51B**, 213 (1996).
- [13] M. Gallagher, *Rydberg Atoms* (Cambridge Univ. Press, Cambridge, 1994).
- [14] K. Yamamoto and S. Matsuki, Nucl. Phys. **72B**, 132 (1999).